NOTES AND CORRESPONDENCE

Estimating Eddy Heat Flux from Float Data in the North Atlantic: The Impact of Temporal Sampling Interval

Brian S. Chinn and Sarah T. Gille

Scripps Institution of Oceanography, La Jolla, California

(Manuscript received 4 October 2005, in final form 13 April 2006)

ABSTRACT

Acoustically tracked float data from 16 experiments carried out in the North Atlantic are used to evaluate the feasibility of estimating eddy heat fluxes from floats. Daily float observations were bin averaged in 2° by 2° by 200-db-deep geographic bins, and eddy heat fluxes were estimated for each bin. Results suggest that eddy heat fluxes can be highly variable, with substantial outliers that mean that fluxes do not converge quickly. If 100 statistically independent observations are available in each bin (corresponding to 500–1000 float days of data), then results predict that 80% of bins will have eddy heat fluxes that are statistically different from zero. Pop-up floats, such as Autonomous Lagrangian Circulation Explorer (ALACE) and Argo floats, do not provide daily sampling and therefore underestimate eddy heat flux. The fraction of eddy heat flux resolved using pop-up float sampling patterns decreases linearly with increasing intervals between float mapping and can be modeled analytically. This implies that flux estimates from pop-up floats may be correctable to represent true eddy heat flux.

1. Introduction

Eddy heat fluxes are thought to be important contributors to the time-mean ocean heat transport (Jayne and Marotzke 2002). However, existing observations provide only a limited view of total eddy heat fluxes. Estimates from satellite data are confined to the surface layer of the ocean and rely on a number of assumptions (Keffer and Holloway 1988; Stammer 1998). Subsurface estimates from current meter data are restricted to the specific locations at which current meters have been deployed (e.g., Wunsch 1999). This paper evaluates the potential for using data from autonomous floats to obtain globally distributed estimates of subsurface eddy heat fluxes.

Global subsurface temperature and velocity observations are now collected as part of the Argo float program (Gould et al. 2004). Here we will use the term "pop-up float" to refer generically to Argo floats, and their predecessors, Autonomous Lagrangian Circulation Explorer (ALACE) floats and Profiling ALACE (PALACE) floats (Davis et al. 1992, 2001). A pop-up float spends most of its time at a predetermined depth below the ocean surface, typically around 1000 m. At predetermined time intervals, typically once every 10 days, it inflates an expandable bladder, which decreases its density, and rises to the ocean surface to transmit via satellite its position as well as subsurface temperature, salinity, and any other data that it may have collected. Pop-up floats are well suited for global measurements, because they operate autonomously, unlike acoustically tracked floats, which require moored sound sources or listening stations.

Pop-up float measurements provide time-averaged velocity information that is useful for tracking the large-scale mean circulation of the ocean (e.g., Davis 1998, 2005). However, since float positions are only determined when the floats rise to the surface, the details of their subsurface trajectories are unknown. This means that they do not resolve high-frequency fluctuations that contribute to eddy motions in the ocean.

Corresponding author address: Sarah Gille, Scripps Institution of Oceanography, 9500 Gilman Dr., Mail Code 0230, La Jolla, CA 92093-0239.
E-mail: sgille@ucsd.edu

DOI: 10.1175/JTECH2057.1

TABLE 1. North Atlantic field programs that collected float data used in this analysis. Here R represents RAFOS, R_I represents RAFOS floats reported to be isopycnal-following in available documentation, S represents SOFAR, and M represents MARVOR. Further information regarding the data themselves is available from the Subsurface Float Data Assembly Center Web site (http://wfdac.whoi.edu).

Expt name	Reference	Year	Type	Floats used
ACCE	Rossby et al. (2001)	1997	R_I	27
ACCEE	Bower et al. (2001)	1996	R_I	58
Canigo	Ambar et al. (2002)	1997	R	20
Eurofloat	Speer et al. (1999)	1996	M	19
Gulf Stream recirculation	Owens (1984)	1980	S	25
Iberian Basin	Rees and Gmitrowicz (1989)	1990	R	33
Local Dynamics Experiment	Rossby et al. (1986b)	1978	S	17
Newfoundland Basin	Schmitz (1985)	1986	S	9
North Atlantic Current	Rossby (1996)	1993	R_I	64
North Atlantic meddies	Richardson et al. (2000)	1993	R	4
Site L	Price et al. (1987)	1982	S	26
Gulf Stream	Schmitz et al. (1981)	1979	S	2
Anatomy (Gulf Stream)	Hummon et al. (1991)	1988	R	9
RAFOS Pilot (Gulf Stream)	Bower and Rossby (1989)	1984	R	26
Synop (Gulf Stream)	Anderson-Fontana and Rossby (1991)	1988	R_I	52
Western Boundary Current	Bower and Hunt (2000a,b)	1994	R_I	2

Richardson (1992) assessed how pop-up floats would undersample eddy kinetic energy (EKE) by analyzing data from acoustically tracked floats in the Gulf Stream region. He compared EKE computed using velocities determined from daily position fixes with EKE determined using velocities time averaged over 15-day or longer periods. Results showed similar EKE spatial patterns for daily and time-averaged velocities, but time-averaged velocities had less than half the EKE of daily velocities.

In this study we carry out an analogous calculation for heat flux. Like Richardson (1992), we make use of acoustically tracked float data from the North Atlantic. Gille (2003) did a similar calculation using temperature and velocity data from Southern Ocean current meters. Her results showed a simple linear relationship between the underestimation of heat flux and the time interval over which velocities and temperatures were averaged. However, results from Eulerian current meters deployed at a few specific locations are not guaranteed to be applicable for Lagrangian measurements collected within a broad range of dynamical regimes.

This analysis has two objectives. The first is to determine how many independent observations are required to obtain heat flux estimates that are statistically different from zero. The second objective is to determine how the heat fluxes obtained from time-averaged pop-up float velocities differ from "true" eddy heat fluxes that could be obtained from acoustically tracked floats and to provide an analytic framework for interpreting these results.

2. Data and methods

This analysis is based on observations from 393 acoustically tracked floats that were part of 16 different field programs carried out between 1978 and 1997, as listed in Table 1. Figure 1 shows float trajectories for the data used in this analysis. All of the float data are archived by the World Ocean Circulation Experiment Subsurface Float Data Assembly Center (http://wfdac.whoi.edu). This study uses floats from the North Atlantic and from depths between 400 and 1000 db, since in this range, the historic database provides a comparatively large number of floats with relatively uniform spatial coverage.

Three types of acoustically tracked floats were used for this study. Sound Fixing and Ranging (SOFAR) floats emit sound pulses that are detected at moored listening stations (Rossby and Webb 1971). RAFOS (opposite of SOFAR) floats listen for sound pulses emitted from moored sound sources and rise to the surface at the end of their deployment period to transmit their time series of position information back to shore via satellite (Rossby et al. 1986a). MARVOR floats resemble RAFOS floats, but are able to rise to the surface to transmit data and redescend to middepth several times during their deployment period (Ollitraut et al. 1994). Float tracking methods have improved since the earliest SOFAR float deployments, and in general the data from the 16 experiments vary in quality. Some of the more recent RAFOS float experiments have used floats that were ballasted to be neutrally buoyant along an isopycnal surface, as indicated in

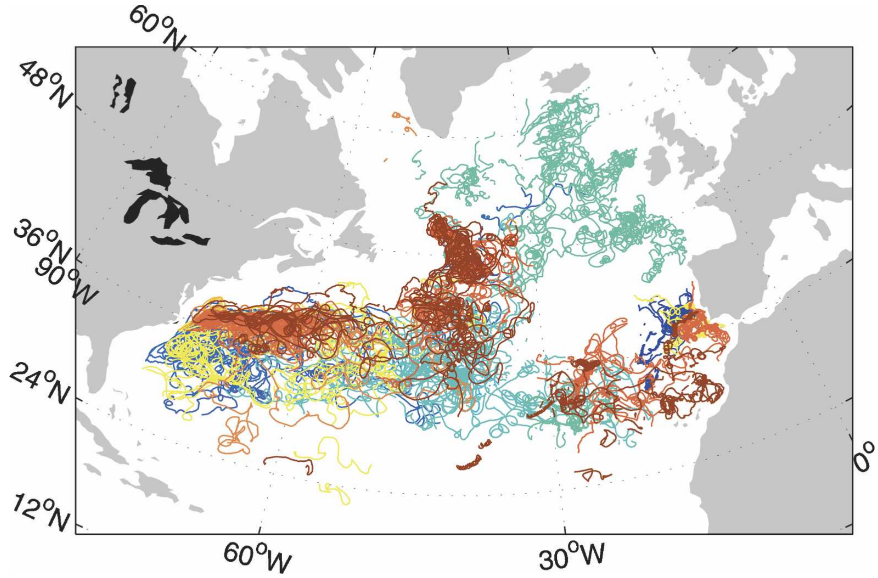

FIG. 1. Trajectories of North Atlantic floats used for this study. All came from experiments listed in Table 1 and operated between 400 and 1000 db. Drifters are color coded by experiment.

Table 1. Although the depths of isopycnal-following floats vary over time, depth differences over an entire float deployment are typically not more than 200 db, the vertical increment used in our data binning. Moreover, LaCasce (2000) and LaCasce and Bower (2000) found no major differences between the statistics of isopycnic and isobaric floats from the North Atlantic. Therefore, in this analysis we combine all available float observations without regard for ballasting method or float design.

All of the floats used in this study were tracked at least once per day (and 45% were tracked more frequently). For this study, once-per-day positions and daily average temperatures were determined for each of the floats. To simulate less frequent pop-up float tracking, velocities and temperatures from acoustically tracked floats were averaged in time. Figure 2 shows a characteristic float track illustrating the effects of the infrequent tracking. As the averaging duration increases, the smoothness of the track diminishes, and several features of the track are lost. For example, the loop made by the float around 30°N and 70.5°W decreases in size at 5- and 10-day averaging and completely disappears at 20-day averaging.

The float data were sorted into 200-db depth bins, since floats are expected to be more energetic at the top of the analysis range at 400 db compared with the bottom at 1000 db. The choice of 200 db was narrow enough to avoid merging data from substantially different depth regimes but sufficiently large to allow statistically meaningful calculations. Potential temperature was computed using a salinity of 34 psu and was referenced to the midpoint of the corresponding 200-db pressure range.

The data were also sorted geographically into 2° latitude by 2° longitude bins. We considered using finer resolution 1° by 1° bins, but found that many bins contained insufficient data to compute robust statistics. We also considered coarser-resolution 5° by 5° bins, but found that we were unable to resolve major oceanographic features at this resolution. The 2° by 2° bins have an average of 258 float days per bin.

Figure 3 shows mean potential temperatures, and Fig. 4 shows mean velocities for each of the three depth ranges. Both the mean temperature and velocity plots clearly resolve large oceanic features such as the Gulf Stream. Velocities tend to decrease with depth and to become less spatially coherent. For example, in the 400–600-db range, the Gulf Stream is evident as a uniform flow that carries water northward along the western boundary and then moves toward the northeast. Between 800 and 1000 db, the uniform structure of the Gulf Stream is less evident, and the flow appears noisy.

3. Computing heat flux

Horizontal eddy heat flux in the ocean can be represented as

$$\langle Q \rangle = \rho C_p \langle \mathbf{u}'\theta' \rangle, \tag{1}$$

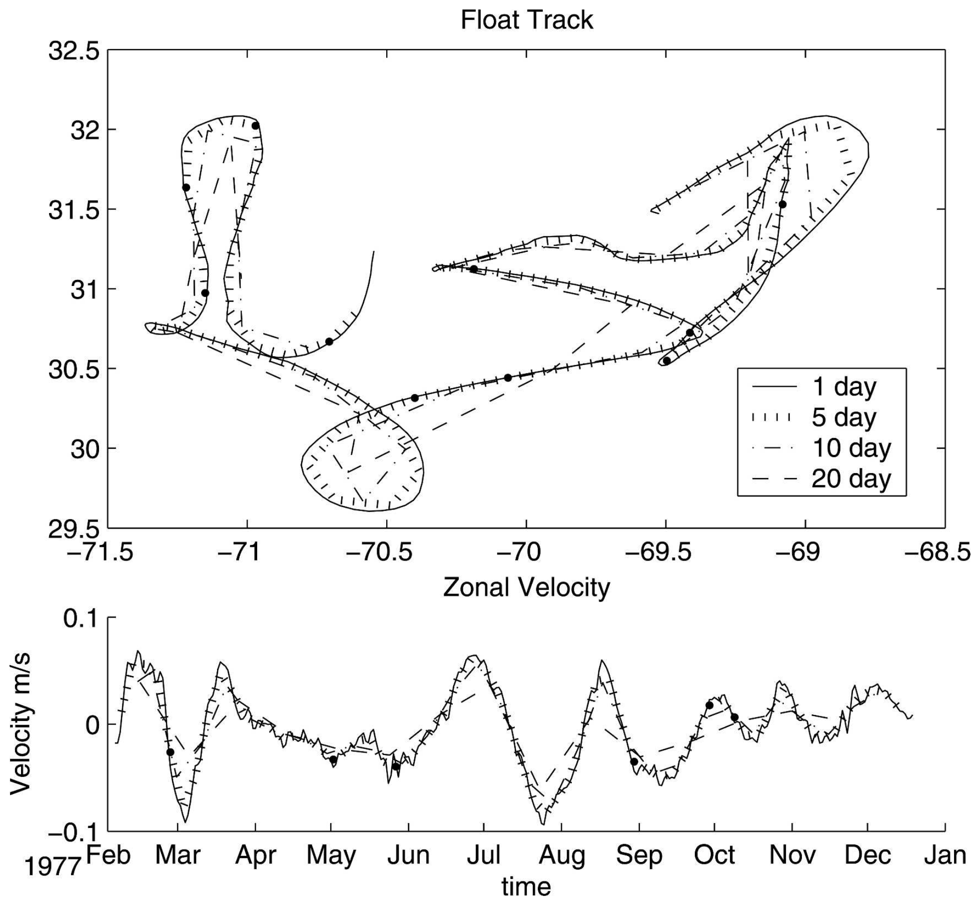

FIG. 2. Effects of infrequent float tracking on the apparent float trajectory. The float in this example was deployed as part of the 1977 Local Dynamics Experiment (LDE).

where here we use $\rho = 1035$ kg m^{-3} as the density of seawater, and $C_p = 4000$ J kg^{-1} °C^{-1} as the specific heat of seawater. The angle brackets $\langle\cdot\rangle$ denote time means, which in this analysis are computed using all observations in a given geographic bin. The horizontal vector velocity anomaly, $\mathbf{u}' = \mathbf{u} - \langle\mathbf{u}\rangle$, is computed for each individual float observation $\mathbf{u}$ relative to the local time-averaged velocity in each bin. The potential temperature anomaly, $\theta' = \theta - \langle\theta\rangle$, is also computed relative to the local bin average.[1]

We examine the eddy heat flux relative to the time-mean streamlines of the flow in the North Atlantic. For this study, the along-stream direction is defined by the bin-averaged mean velocities, and the cross-stream direction is 90° to the left of the along-stream direction. We also tested using dynamic topography computed from atlas data (Conkright et al. 2002) to determine the direction of the mean flow, but found this to produce noisier results. In the region of the Gulf Stream, the along-stream component represents the eddy heat flux carried by the mean Gulf Stream, and the cross-stream component represents the net flux northward across the Gulf Stream. In a simplified framework, if one imagines that the circulation at any given depth in the North Atlantic recirculates without changing depth, then the cross-stream component of heat flux might be thought of as controlling net poleward heat transport, while the along-stream component drives a recirculation and will not produce a net heat transport. The cross-stream component is therefore more analogous to the divergent heat flux discussed by Marshall and Shutts (1981), and is most relevant for understanding the net heat flux divergence.

Bin-averaged eddy heat fluxes (not shown) are on the order of 100 kW m^{-2}, though outliers can sometimes be much larger. Overall the eddy heat flux esti-

[1] Bauer et al. (2002) used an alternative approach (not explored here) in which the time mean is a smoothed spatially varying field. Their strategy avoids potential biases in regions of strong spatial gradients, but implicitly assumed that eddy and mean processes are distinguishable.

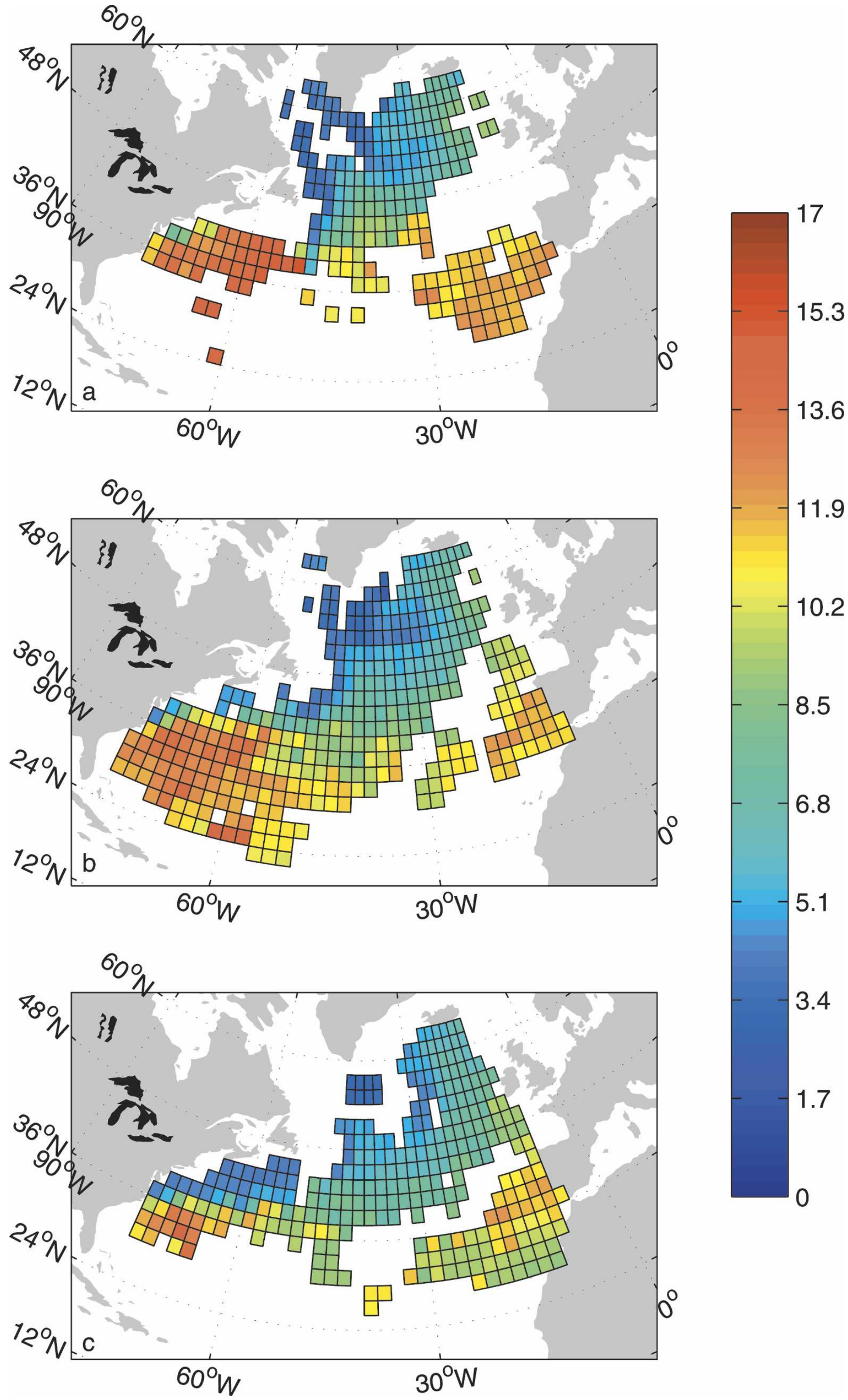

FIG. 3. Mean float temperatures, bin averaged in 2° by 2° geographic bins and sorted by depth with (a) 400–600-, (b) 600–800-, and (c) 800–1000-db measurements.

mates obtained from floats are of the same magnitude as fluxes obtained from moored temperature and current meter records from the North Atlantic (Wunsch 1999) and also show similar spatial patterns. Within statistical error bars (see below for computational details), the mean along-stream eddy heat flux is positive at all depths and averaging durations. Peak along-stream heat fluxes occur within the Gulf Stream region

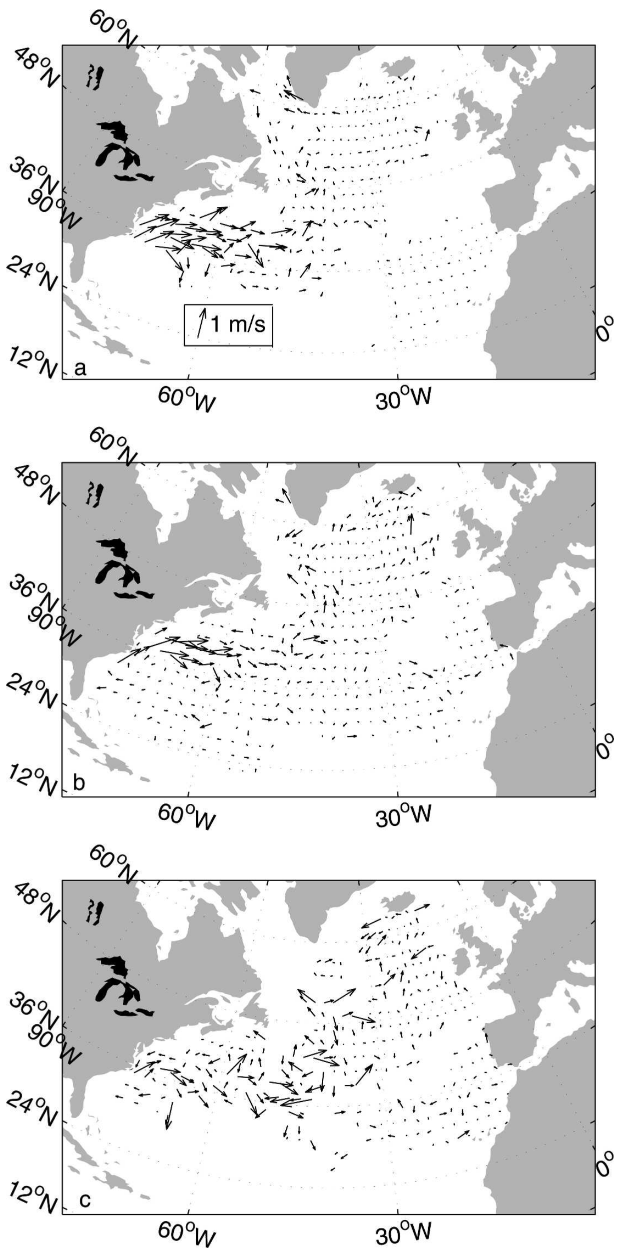

FIG. 4. Mean float velocities, as in Fig. 3.

and attenuate with depth. Outside the Gulf Stream, along-stream heat fluxes are small and often not significantly different from zero. Compared with along-stream fluxes, cross-stream eddy heat fluxes are typically smaller and less depth dependent. They also show no predominant sign and indicate a less pronounced difference between the Gulf Stream and the rest of the North Atlantic than do along-stream fluxes.

Since eddy heat fluxes vary with depth and position, in each bin, we demeaned the individual eddy heat flux estimates and normalized them by the local standard deviation to produce a normalized measure Q^* of heat flux variability:

$$Q^* = \frac{u'\theta' - \langle u'\theta' \rangle}{\sigma}, \tag{2}$$

where the standard deviation $\sigma = \sqrt{\langle (u'\theta' - \langle u'\theta' \rangle)^2 \rangle}$. This normalization allows us to combine observations from disparate regions to generate a single probability density function (PDF) (Fig. 5), showing the likelihood of observing a heat flux event that is extreme relative to the local mean. The PDF of Q^* is peaked in the center and is broader than either the Gaussian or double exponential distributions (also shown in Fig. 5). The broad tails of the PDF indicate that eddy heat fluxes can be very large, and the mean of a finite number of observations can be strongly influenced by one or two large events. In the composite distribution in Fig. 5, the mean and median both converge to zero. In section 4, we use the median as a measure of the typical heat flux in each bin, because it is less strongly influenced by outliers in bins where only a few observations are available.

How many independent observations are required to obtain eddy heat flux estimates that differ statistically from zero? For each bin, we assume that the statistical uncertainty of the mean quantity $\langle u'\theta' \rangle$ is the standard deviation of $u'\theta'$, σ, divided by $\sqrt{N_e}$, where N_e is the number of effective degrees of freedom; N_e is less than the total number of observations N available in the bin, because consecutive observations are correlated. The number of independent degrees of freedom in the float data depends on the temporal decorrelation scale τ. The autocorrelation is

$$R(k) = \frac{1}{\sum_{i=1}^{n} u_i'^2} \sum_{i=1}^{n-k} u_i' u_{i+k}'. \tag{3}$$

This function was calculated for each of the time series and averaged to produce the mean autocorrelation function for each geographic bin. The decorrelation time was calculated as the first zero crossing of $\langle R(k) \rangle$.

Average decorrelation times for 400 to 1000 db are between 5 and 10 days (see Table 2), with temperature decorrelating more slowly than either of the velocity components. These estimates are similar to previous estimates, which have placed decorrelation times at approximately 3–5 (Zhang et al. 2001) or 10 days (Owens 1991). Decorrelation times seem to correspond with the local standard deviation (not shown): areas with high σ generally have shorter decorrelation scales than do areas with low σ.

This means that a statistically significant eddy heat

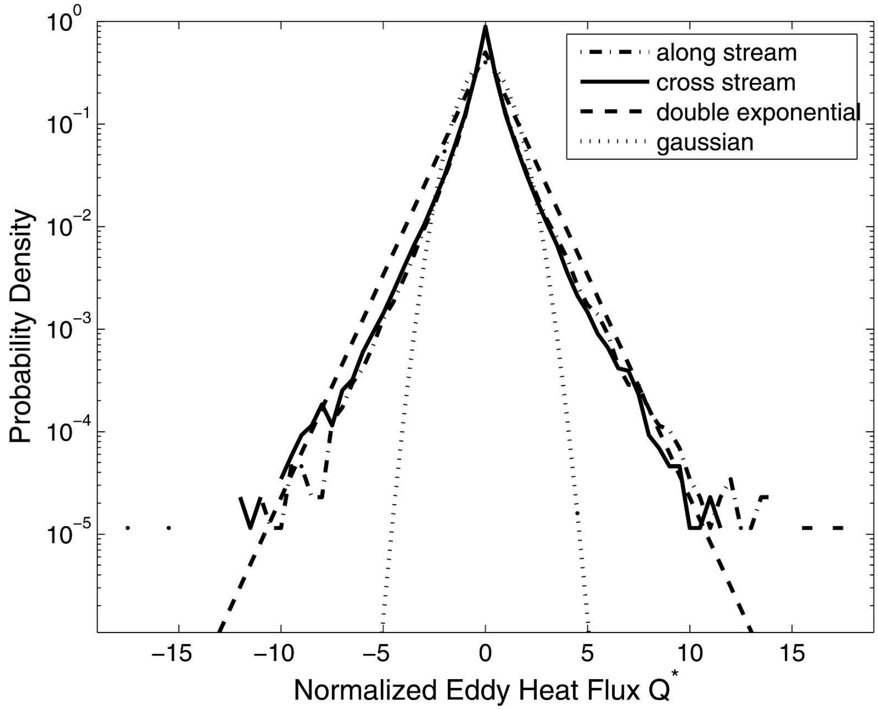

FIG. 5. Probability density function of normalized eddy heat fluxes Q^*. Double exponential and Gaussian PDFs are also shown for comparison.

flux estimate will require that the number of statistically independent observations N_e exceed $\sigma^2/\langle u'\theta'\rangle^2$, where $N_e = N\delta t/\tau$, δt is the interval between observations, and $\tau/\delta t$ is the number of observations collected during the decorrelation time period. The North Atlantic float records include some float pairs that were within 15 km of each other at some point during their deployment (LaCasce and Bower 2000). These pairs represent a comparatively small fraction of the overall dataset, and in contrast with Owens (1991), in the calculations presented here, we have not attempted to adjust the number of degrees of freedom to account for these possible overlapping samples. Eddy heat flux estimates are often small or not statistically different from zero, as Wunsch (1999) also noted. In some cases, even large mean fluxes may not be statistically different from zero. Table 3 shows the number of bins at each depth, and the fraction of these bins with along-stream eddy heat fluxes that are statistically different from zero.

Figure 6 shows the cumulative distribution of the fraction of geographic bins with statistically significant eddy heat fluxes as a function of the number of statistically independent data points per bin. Here results from all three depth ranges and from both along-stream and cross-stream heat fluxes have been merged. A minimum of 100 statistically independent observations are required in order to obtain statistically nonzero eddy heat fluxes in 80% of the bins. If we assume a decorrelation time scale of 5 to 10 days, then this implies that 500 to 1000 float days of observations are required in each geographic bin. If we wanted to obtain statistically nonzero eddy heat fluxes in 90% of the geographic bins, then nearly 500 statistically independent observations per bin (or 2500 to 5000 float days of observation) would be required. This calculation de-

TABLE 2. Mean and standard deviation of decorrelation times in days. Statistics are computed from means of all geographic bins; local values are used in calculation.

	Decorrelation time	Std dev
Temperature	9.4	9.2
Zonal velocity	6.1	5.4
Meridional velocity	5.9	4.9

TABLE 3. Number of bins in each depth range and fraction of bins having along-stream eddy heat fluxes that are statistically insignificant or that do not fall within error bars of zero.

Depth range (db)	Total bins	Percent significant
400–600	250	73.2
600–800	359	78.0
800–1000	293	79.2

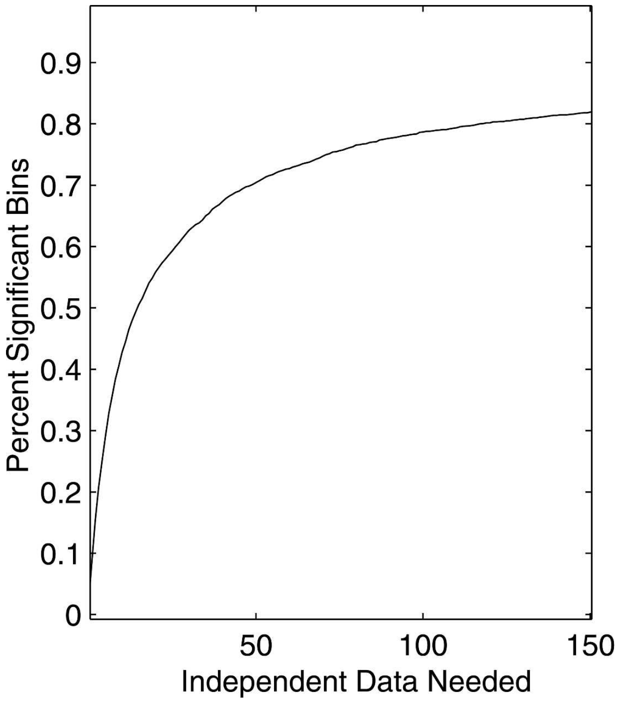

FIG. 6. Cumulative distribution function indicating the number of statistically independent observations required in each bin in order to obtain eddy heat fluxes that are statistically different from zero.

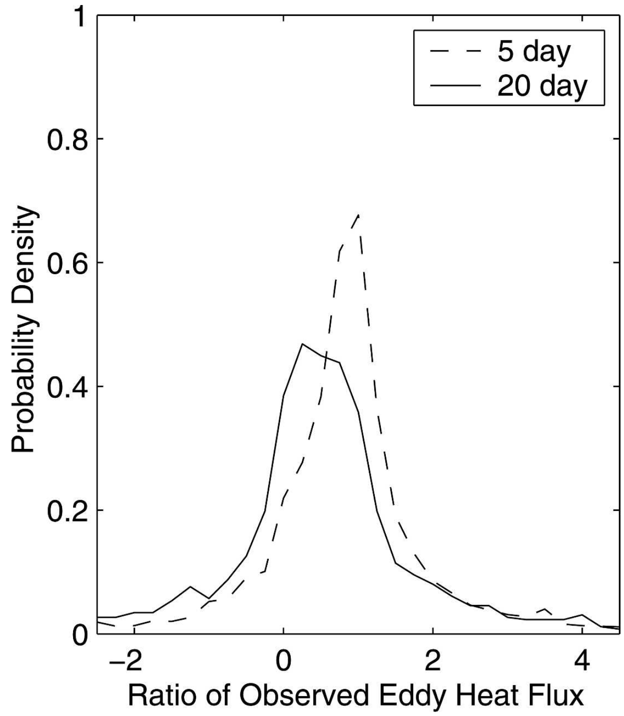

FIG. 7. PDF of observed eddy heat flux ratios $r_{5\ \mathrm{day}}$ and $r_{20\ \mathrm{day}}$. Ratios compare 5- and 20-day averages with unaveraged data. Ratios based on 5-day averages have a mean of 0.65, a median of 0.82, and a standard deviation of 26.32. For the 20-day averages, the mean ratio is 0.15, the median is 0.49, and the standard deviation is 50.59.

pends on a large extrapolation, since on average bins have fewer than 300 float days, and therefore results must be used carefully.

4. Evaluating eddy heat flux from pop-up floats

Each float trajectory was time averaged into 2-, 5-, 10-, 15-, and 20-day increments to simulate pop-up floats operating at different recording intervals. We found that if we averaged data over time periods longer than 20 days, we had few observations in each bin and, as a result, the statistical uncertainties were large relative to the means in each bin. We computed eddy heat fluxes in each geographic bin using the 2–20-day time-averaged temperature and velocity estimates to represent the instantaneous temperature and velocity. The resulting heat fluxes vary substantially relative to the "true" heat fluxes computed from data collected at 1-day increments. When float data are averaged to duplicate pop-up float sampling, eddy heat fluxes change in much the same way that Richardson (1992) showed EKE to change. As averaging duration increases the size of pockets of significant eddy heat flux and their maximum values are reduced.

To quantify the effect of multiday sampling, for each pressure range and time averaging interval, we computed the ratio of the observed eddy heat flux:

$$r_{n\ \mathrm{day}} = \frac{\langle u'\theta' \rangle_{n\ \mathrm{day}}}{\langle u'\theta' \rangle_{1\ \mathrm{day}}}. \tag{4}$$

Figure 7 shows the PDF of the flux ratios $r_{5\ \mathrm{day}}$ and $r_{20\ \mathrm{day}}$. Here the ratios were computed for each individual drifter in each geographic bin, and tracks for which only one n-day segment was available were omitted. At 5 days the distribution is centered near one and the mean and median are relatively close, and maintain the same sign. However, the PDF of $r_{20\ \mathrm{day}}$ is broader, and the mean differs from the median. The mean values are strongly influenced by large outlying values, and as noted in section 3, we take medians to be representative of typical heat fluxes in each bin.

For each of the three depth ranges, the overall bin median values of observed eddy heat flux γ were calculated:

$$\gamma(n) = \mathrm{median}(r_{n\ \mathrm{day}}). \tag{5}$$

Figure 8, which shows $\gamma(n)$ for cross-stream and along-stream eddy heat fluxes at all depth ranges, was gener-

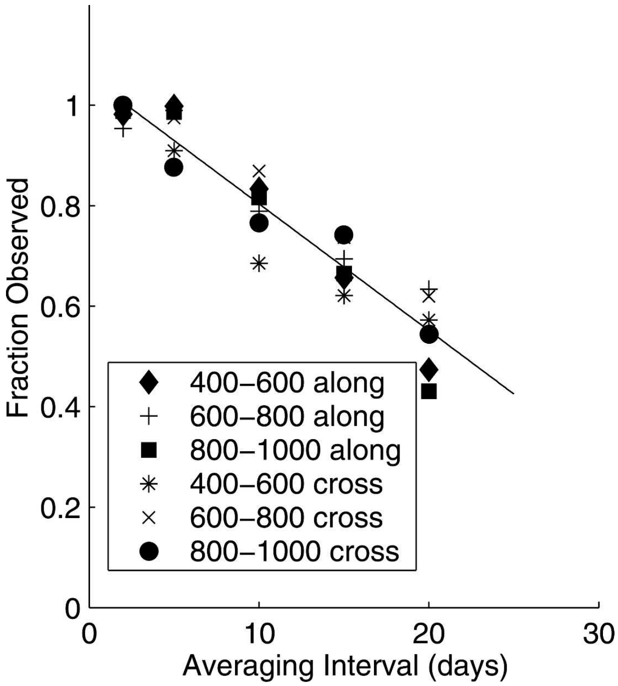

FIG. 8. Median observed eddy heat flux ratios $\gamma(n)$ for along-stream and cross-stream eddy heat flux estimates in three depth ranges.

ated using only bins with statistically significant eddy heat fluxes. The solid black line is the least squares fit through the data:

$$\tilde{\gamma}(n) = (-0.0252 \pm 0.0015) \times n + 1.056 \pm 0.019, \tag{6}$$

where $\tilde{\gamma}$ is the fitted median ratio, n is the averaging time in days, and uncertainties represent 95% confidence intervals. Though the available data do not allow analysis for durations longer than 20 days, we expect that the linear decrease cannot continue indefinitely and that the curve will eventually asymptote to a constant value of heat flux ratio.

Temporal averaging has two main effects on the uncertainties in the calculations. First, it significantly decreases the quantity of data available. Although using time-averaging intervals shorter than the decorrelation time does not formally reduce the number of independent samples available, using longer time-averaging intervals does reduce the number of independent samples and correspondingly the spatial coverage of the eddy heat flux results. Second, in many cases standard errors decrease as sampling interval grows. Time averaging acts like a low-pass filter, reducing the impact of isolated large outliers and in turn reducing the variance of the eddy heat flux estimates.

5. Analytic solution

The linear trend in Fig. 8 suggests that we may be able to find a simple model to represent the eddy heat flux ratios. Since eddy heat flux depends on the correlation between velocity and temperature fluctuations, we can define temperature as $\theta(t) = su(t) + n(t)$, where s is a constant, and n represents the portion of the temperature signal that is uncorrelated with velocity.

Velocity u and temperature θ are both assumed to have red spectra, except at very low frequencies. For frequencies exceeding $\pm f_0$, their Fourier transforms can be represented as

$$\hat{u} = a|f|^{-\alpha}e^{i\phi(f)} + \hat{n}_u, \tag{7}$$

$$\hat{\theta} = b|f|^{-\beta}e^{i\phi(f)} + \hat{n}_\theta, \tag{8}$$

where the caret $\hat{}$ represents the Fourier transform (in frequency), f is frequency, α and β are constants representing the spectral slopes for velocity and potential temperature, respectively, and $\phi(f)$ represents the frequency-dependent phase of the Fourier transform. The Fourier transform of the noise n has been divided into a velocity component $\hat{n}_u$ and a temperature component $\hat{n}_\theta$, which are assumed to be incoherent. Eddy heat fluxes depend on the correlation between velocity and temperature. Here, in order to focus on correlated portions of the signals, we specify that $\hat{u}$ and $\hat{\theta}$ have the same phase, but we allow $\phi(f)$ to vary arbitrarily with frequency. The Fourier transform of the eddy heat flux $\widehat{u'\theta'}$ is the convolution of the Fourier transforms $\hat{u}$ and $\hat{\theta}$:

$$\widehat{u'\theta'}\,(f') = \int_{-\infty}^{\infty} \hat{u}(f)\hat{\theta}(f - f')^*\, df, \tag{9}$$

where an asterisk denotes the complex conjugate.

Since a pop-up float measurement represents an average over several days, it can be thought of as the true velocity and temperature, filtered with a box-car filter h of width L. In the frequency domain, this is equivalent to multiplying the Fourier transforms $\hat{u}$ and $\hat{\theta}$ by $\mathrm{sinc}(\pi f L)$. The Fourier transform of the eddy heat flux determined from time-averaged quantities is

$$\widehat{u_n'\theta_n'}\,(f') = \int_{-\infty}^{\infty} \hat{u}(f)\hat{\theta}(f - f')^*\hat{h}(f)\hat{h}(f - f')^*\, df = \int_{-\infty}^{\infty} \hat{u}(f)\hat{\theta}(f - f')^* \frac{\sin(\pi f L)}{\pi f L}\frac{\sin(\pi(f - f')L)}{\pi(f - f')L}\, df, \tag{10}$$

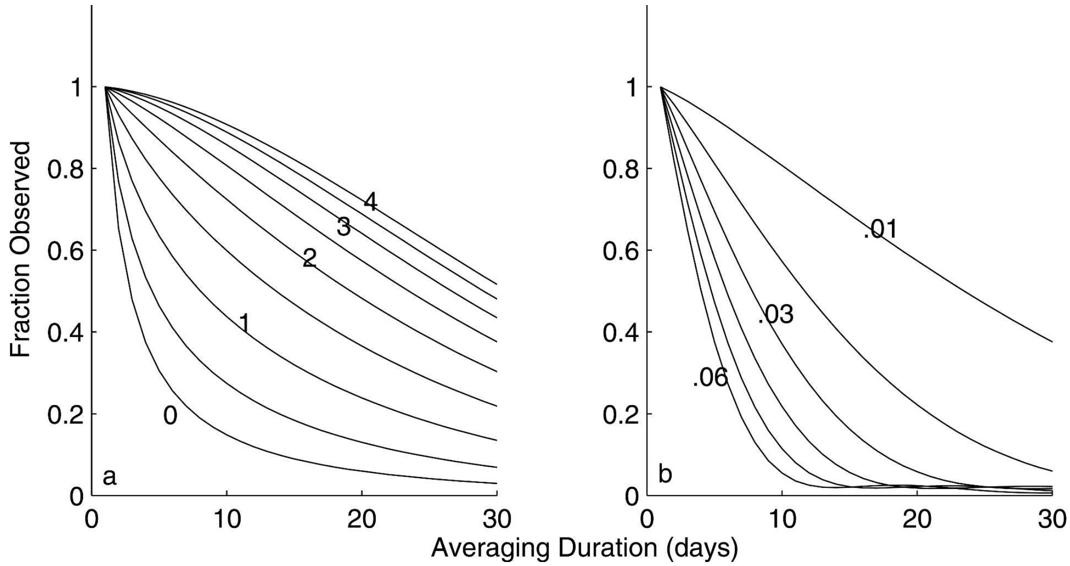

FIG. 9. Analytic solutions for eddy heat flux ratios. (a) Fraction observed plotted as a function of averaging duration, with spectral slopes $\alpha + \beta$ ranging from 0 to 4 in increments of 0.5 and f_0 set to 0.01. (b) Fraction observed with f_0 ranging from 0.01 to 0.06 with spectral slope set to 2.5.

where the subscript n indicates averages over n days.

Since we are interested in the time-mean eddy heat flux, we consider only the zero frequency component, when $f' = 0$, which will represent the mean (multiplied by a scaling factor proportion to the duration of the time series). The "true" eddy heat flux can be inferred from

$$\langle u'\theta'\rangle = \widehat{u'\theta'}(0) = 2\int_{f_0}^{\infty} abf^{-\alpha-\beta}\,df, \tag{11}$$

and the pop-up float approximation is

$$\langle u_n'\theta_n'\rangle = \widehat{u_n'\theta_n'}(0) = 2\int_{f_0}^{\infty} abf^{-\alpha-\beta}\frac{\sin^2(\pi fL)}{\pi^2 f^2 L^2}\,df. \tag{12}$$

Here we have assumed that the mean ($f = 0$) has been removed from the data, and that nonzero frequency components below f_0 do not contribute to the eddy heat flux.

The integral (12) can be written

$$\begin{aligned}\langle u_n'\theta_n'\rangle &= \frac{2ab}{\pi^2L^2}\int_{f_0}^{\infty} f^{-\alpha-\beta-2}\sin^2(\pi fL)\,df = \frac{ab}{\pi^2L^2}\int_{2\pi f_0L}^{\infty}\left(\frac{x}{2\pi L}\right)^{-\alpha-\beta-2}[1-\cos(x)]\frac{dx}{2\pi L} = 4ab(2\pi L)^{\alpha+\beta-1}\\ &\times\left\{\frac{(2\pi f_0L)^{-\alpha-\beta-1}}{\alpha+\beta+1} - \frac{1}{2}\left[\exp\left(\frac{i\pi(\alpha+\beta+1)}{2}\right)\Gamma(-\alpha-\beta-1, i2\pi f_0L)\right.\right.\\ &\left.\left.+\exp\left(\frac{i\pi(\alpha+\beta+1)}{2}\right)\Gamma(-\alpha-\beta-1, -i2\pi f_0L)\right]\right\},\end{aligned} \tag{13}$$

where Γ is the incomplete gamma function. Both the first and second terms are proportional to L^{-2} and cancel to leading order.

Estimates of the eddy heat flux do not depend on the individual slopes α or β, but only on their sum. Figure 9 shows the ratio $\langle u_n'\theta_n'\rangle/\langle u'\theta'\rangle$ as a function of L for a range of different total spectral slopes. The ratio is nearly linear when $\alpha + \beta$ is approximately two. Spectra computed from Eulerian measurements typically have slopes around 3 for velocity and 2 for temperature, implying $\alpha \approx 1.5$ and $\beta \approx 1$ (Wunsch 1981). For Lagrangian velocities from 700-m-depth floats, Rupolo et al. (1996) showed a similar structure; the spectra are flat at low frequencies and have a slope of approximately 3 for high frequencies. Spectra from the data used in this analysis have similar shapes and slopes, implying that $\alpha + \beta$ should be between 2 and 3.

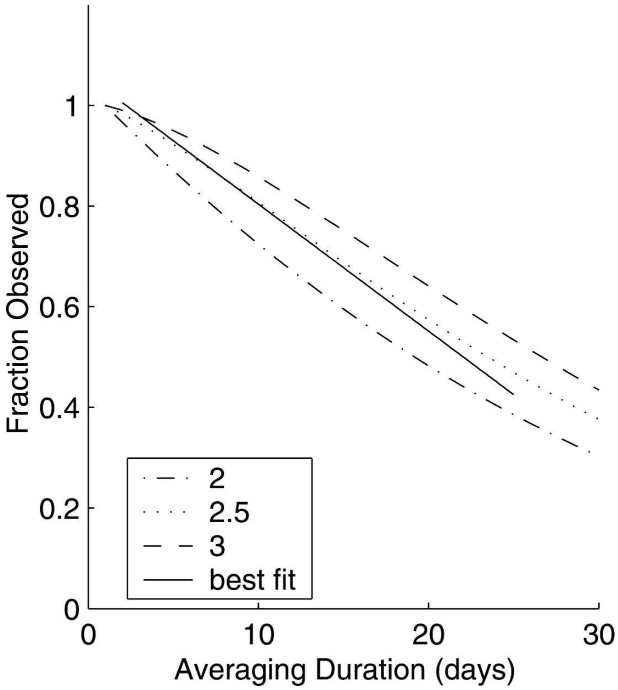

FIG. 10. Predictions for eddy heat flux ratios calculated using analytic solution, using $\alpha + \beta = 2$, 2.5, and 3, and $f_0 = 0.01$. The linear fit to observations is also plotted.

Figure 9b shows that changes in f_0 change the slope of the curves as a function of L, but they do not change the basic shapes of the curves. We find a close match to observation results when we use $f_0 = 0.01$ and $\alpha + \beta = 2.5$, as shown in Fig. 10.

6. Summary and conclusions

This study has focused on eddy heat flux estimates from RAFOS, SOFAR, and MARVOR floats deployed in the North Atlantic. Eddy heat fluxes vary horizontally and vertically in the North Atlantic with typical values on the order of 100–200 kW m^{-2}. The largest patches of nonzero eddy heat flux are consistently located in the Gulf Stream. However, eddy heat fluxes have non-Gaussian distributions with large tails, making their means slow to converge. In many cases the statistical uncertainty exceeds the actual observed eddy heat flux. These large uncertainties make difficult detailed evaluation of the vertical and spatial structure of eddy heat fluxes.

These results show that on average pop-up floats tend to underestimate true eddy heat fluxes. While the exact impact of pop-up float sampling depends on a number of factors including depth and geographic region, the median ratio of resolved to total eddy heat flux decreases linearly with increasing time-averaging interval, and this effect can be well modeled by assuming that velocity and temperature both have coherent red spectra with spectral slopes between 2 and 3.

Approximately 100 statistically independent observations are required to determine statistically significant eddy heat flux estimates in 80% of geographic bins. Given that ALACE, PALACE, and Argo floats sample at times ranging from 10 and 25 days, this implies between 3 and 7 yr of pop-up float tracks would be necessary in every bin in order to obtain realistic global heat flux estimates.

Acknowledgments. Discussions with Colm Caulfield and Stefan Llewellyn Smith have helped to refine the presentation of these results and particularly the analytic solution in section 5. The reviewers' comments also helped clarify the paper. This research was supported by the National Science Foundation under Grant OCE-9985203/OCE-0049066.

REFERENCES

Ambar, I., N. Serra, S. Sadoux, and D. Renourd, 2002: Observations and laboratory modeling of meddy generation at Cape St. Vincent. *J. Phys. Oceanogr.,* **32,** 3–25

Anderson-Fontana, S., and T. Rossby, 1991: RAFOS floats in the SYNOP experiment 1988–1990. G.S.O. Tech. Rep., 91-7, University of Rhode Island, 155 pp.

Bauer, S., M. S. Swenson, and A. Griffa, 2002: Eddy mean flow decomposition and eddy diffusivity estimates in the tropical Pacific Ocean: 2. Results. *J. Geophys. Res.,* **107,** 3154, doi:10.1029/2000JC000613.

Bower, A. S., and T. Rossby, 1989: Evidence of cross-frontal exchange processes in the Gulf Stream based on isopycnal RAFOS float data. *J. Phys. Oceanogr.,* **19,** 1177–1190.

——, and H. D. Hunt, 2000a: Lagrangian observations of the deep western boundary current in the North Atlantic Ocean. Part I: Large-scale pathways and spreading rates. *J. Phys. Oceanogr.,* **30,** 764–783.

——, and ——, 2000b: Lagrangian observations of the deep western boundary current in the North Atlantic Ocean. Part II: The Gulf Stream–deep western boundary current crossover. *J. Phys. Oceanogr.,* **30,** 784–804.

——, H. H. Furey, and P. L. Richardson, 2001: Warm water pathways in the northeastern North Atlantic: ACCE RAFOS float data report, November 1996–November 1999. WHOI Tech. Rep., 2001-17, 161 pp.

Conkright, M. E., R. A. Locarnini, H. E. Garcia, T. D. O'Brien, T. P. Boyer, C. Stephens, and J. I. Antonov, 2002: World Ocean Atlas 2001: Objective analyses, data statistics, and figures. CD-ROM Doc., NODC Internal Rep. 17, 17 pp. [Available online at http://nodc.noaa.gov/OC5/WOA01/readme.pdf.]

Davis, R. E., 1998: Preliminary results from directly measuring middepth circulation in the tropical and South Pacific. *J. Geophys. Res.,* **103,** 24 619–24 639.

——, 2005: Intermediate-depth circulation of the Indian and

South Pacific Oceans measured by autonomous floats. *J. Phys. Oceanogr.,* **35,** 683–707.

——, D. C. Webb, L. A. Regier, and J. Dufour, 1992: The autonomous Lagrangian circulation explorer (ALACE). *J. Atmos. Oceanic Technol.,* **9,** 264–285.

——, J. T. Sherman, and J. Dufour, 2001: Profiling ALACEs and other advances in autonomous subsurface floats. *J. Atmos. Oceanic Technol.,* **18,** 982–993.

Gille, S. T., 2003: Float observations of the Southern Ocean. Part II: Eddy fluxes. *J. Phys. Oceanogr.,* **33,** 1182–1196.

Gould, J., and Coauthors, 2004: Argo profiling floats bring new era of in situ ocean observations. *Eos, Trans. Amer. Geophys. Union,* **85,** 179, 190–191.

Hummon, J., T. Rossby, E. Carter, J. Lillibridge III, M. Liu, K. Schultz Tokos, S. Anderson-Fontana, and A. Mariano, 1991: The anatomy of Gulf Stream meanders. Vol. I: Technical description and fall cruise data. G.S.O. Tech. Rep. 91-4, University of Rhode Island, 246 pp.

Jayne, S. R., and J. Marotzke, 2002: The oceanic eddy heat transport. *J. Phys. Oceanogr.,* **32,** 3328–3345.

Keffer, T., and G. Holloway, 1988: Estimating Southern Ocean eddy flux of heat and salt from satellite altimetry. *Nature,* **332,** 624–626.

LaCasce, J. H., 2000: Floats and f/H. *J. Mar. Res.,* **58,** 61–95.

——, and A. Bower, 2000: Relative dispersion in the subsurface North Atlantic. *J. Mar. Res.,* **58,** 863–894.

Marshall, J., and G. Shutts, 1981: A note on rotational and divergent eddy fluxes. *J. Phys. Oceanogr.,* **11,** 1677–1680.

Ollitraut, M., G. Loaec, and C. Dumortier, 1994: MARVOR: A multicycle RAFOS float. *Sea Technol.,* **35,** 39–44.

Owens, W. B., 1984: A synoptic and statistical description of the Gulf Stream and subtropical gyre using SOFAR floats. *J. Phys. Oceanogr.,* **14,** 104–113.

——, 1991: A statistical description of the mean circulation and eddy variability in the northwestern Atlantic using SOFAR floats. *Progress in Oceanography,* Vol. 28, Pergamon Press, 257–303.

Price, J. F., T. K. Mckee, and J. R. Valdes, 1987: Site 1 SOFAR float experiment 1982–1985. WHOI Tech. Rep. WHOI-87-52, 289 pp.

Rees, J. M., and E. M. Gmitrowicz, 1989: Dispersion measurements from SOFAR floats on the Iberian abyssal plain. *Interim Oceanographic Description of the North-East Atlantic Site for the Disposal of Low-Level Radioactive Waste,* Vol. 3, F. Nyffeler and W. Simmons, Eds., Nuclear Energy Agency/OECD, 64–67.

Richardson, P. L., 1992: Velocity and eddy kinetic energy of the Gulf Stream system from 700-m SOFAR floats subsampled to simulate pop-up floats. *J. Atmos. Oceanic Technol.,* **9,** 495–503.

——, A. S. Bower, and W. Zenk, 2000: A census of Meddies tracked by floats. *Progress in Oceanography,* Vol. 45, Pergamon Press, 209–250.

Rossby, T., 1996: The North Atlantic current and surrounding waters: At the crossroads. *Rev. Geophys.,* **34,** 463–481.

——, and D. Webb, 1971: The four month drift of a Swallow float. *Deep-Sea Res.,* **18,** 1035–1039.

——, D. Dorson, and J. Fontaine, 1986a: The RAFOS system. *J. Atmos. Oceanic Technol.,* **3,** 672–679.

——, J. Price, and D. Webb, 1986b: The spatial and temporal evolution of a cluster of SOFAR floats in the POLYMODE local dynamics experiment (lde). *J. Phys. Oceanogr.,* **16,** 428–442.

——, S. Anderson-Fontana, P. Lazarevich, P. Perez-Brunius, M. Prater, and H.-M. Zhang, 2001: RAFOS float data report of the Atlantic Climate Change Experiment (ACCE) 1997–2000. G.S.O. Tech. Rep., 2001-4, University of Rhode Island, 112 pp.

Rupolo, V., B. L. Hua, A. Provenzale, and V. Artale, 1996: Lagrangian velocity spectra at 700 m in the western North Atlantic. *J. Phys. Oceanogr.,* **26,** 1591–1607.

Schmitz, W. J., Jr., 1985: SOFAR float trajectories associated with the Newfoundland Basin. *J. Mar. Res.,* **43,** 761–778.

——, J. F. Price, P. L. Richardson, W. B. Owens, D. C. Webb, R. E. Cheney, and H. T. Rossby, 1981: A preliminary exploration of the Gulf Stream system with SOFAR floats. *J. Phys. Oceanogr.,* **11,** 1194–1204.

Speer, K. G., J. Gould, and J. H. LaCasce, 1999: Year-long float trajectories in the Labrador Sea water of the eastern North Atlantic. *Deep-Sea Res. II,* **46,** 165–179.

Stammer, D., 1998: On eddy characteristics, eddy transports, and mean flow properties. *J. Phys. Oceanogr.,* **28,** 727–739.

Wunsch, C., 1981: Low-frequency variability of the sea. *Evolution of Physical Oceanography,* B. A. Warren and C. Wunsch, Eds., MIT Press, 342–375.

——, 1999: Where do ocean eddy heat fluxes matter? *J. Geophys. Res.,* **104,** 13 235–13 249.

Zhang, H. M., M. D. Prater, and T. Rossby, 2001: Isopycnal Lagrangian statistics from the North Atlantic Current RAFOS float observations. *J. Geophys. Res.,* **106,** 13 817–13 836.